Behavior of Flow over Step Orography

WILLIAM A. GALLUS JR.

Department of Geological and Atmospheric Sciences, Iowa State University, Ames, Iowa

JOSEPH B. KLEMP

National Center for Atmospheric Research, Boulder, Colorado

(Manuscript received 16 February 1999, in final form 12 May 1999)

ABSTRACT

A two-dimensional nonhydrostatic version of the NCEP regional Eta Model together with analytic theory are used to examine flow over isolated mountains in numerical simulations using a step-terrain vertical coordinate. Linear theory indicates that a singularity arises in the steady flow over the step corners for hydrostatic waves and that this discontinuity is independent of height. Analytic solutions for both hydrostatic and nonhydrostatic waves reveal a complex behavior that varies with both horizontal and vertical resolution.

Witch of Agnessi experiments are performed with a 2D version of the Eta Model over a range of mountain half-widths. The simulations reveal that for inviscid flow over a mountain using the step-terrain coordinate, flow will not properly descend along the lee slope. Rather, the flow separates downstream of the mountain and creates a zone of artificially weak flow along the lee slope. This behavior arises due to artificial vorticity production at the corner of each step and can be remedied by altering the finite differencing adjacent to the step to minimize spurious vorticity production.

In numerical simulations with the step-terrain coordinate for narrow mountains where nonhydrostatic effects are important, the disturbances that arise at step corners may be of the same horizontal scale as those produced by the overall mountain, and the superposition of these disturbances may reasonably approximate the structure of the continuous mountain wave. For wider mountains, where perturbations are nearly hydrostatic, the disturbances above the step corners have horizontal scales that are much smaller than the overall scale of the mountain and appear as sharp spikes in the flow field. The deviations from the ''classic'' Witch of Agnesi solution are significant unless the vertical resolution is very small compared to the height of the mountain. In contrast, simulations with the terrain-following vertical coordinate produce accurate solutions provided the vertical grid interval is small compared to the vertical wavelength of the mountain waves (typically at least an order of magnitude larger than the mountain height).

1. Introduction

Terrain-following vertical coordinates (cf. Phillips 1957; Gal-Chen and Somerville 1975) have been used extensively to accommodate orography in models for atmosphere flow. However, Mesinger and Janjic (1985), among others, have found that errors in computing the horizontal pressure gradient force in models using a terrain-following vertical coordinate can be substantial in the vicinity of steep topography. To minimize this error, models using step-terrain profiles (Mesinger 1984) have been introduced, such as the National Centers for Environmental Prediction (NCEP) regional Eta Model (e.g., Mesinger et al. 1988; Janjic 1990, 1994). In that model, the topography can be represented as discrete steps whose tops coincide exactly with the nearly horizontal coordinate surfaces (see Fig. 1, from Black 1994). With the continuing increase in computational resources, operational models like the Eta Model are being run at successively finer resolutions. A nonhydrostatic version of the Eta Model was developed (Gallus and Rancic 1996) and tested successfully in benchmark thermal bubble experiments. The vertical coordinate in the nonhydrostatic version switched from a function of pressure (used in the hydrostatic version) to a function of height (Eta-z).

Although mountain-induced gravity waves are relatively unimportant at typical resolutions used operationally in the past, these perturbations can play a significant role in atmospheric motion as the horizontal resolution approaches or exceeds $O(10)$ km. Therefore, it is important to understand the behavior of step-terrain models in generating gravity wave motion within flow over mountainous terrain. In this paper, we shall examine the effect of the step-terrain approximation on

Corresponding author address: Dr. William A. Gallus Jr., Department of Geological and Atmospheric Sciences, Iowa State University, 3025 Agronomy Hall, Ames, IA 50011.
E-mail: wgallus@iastate.edu

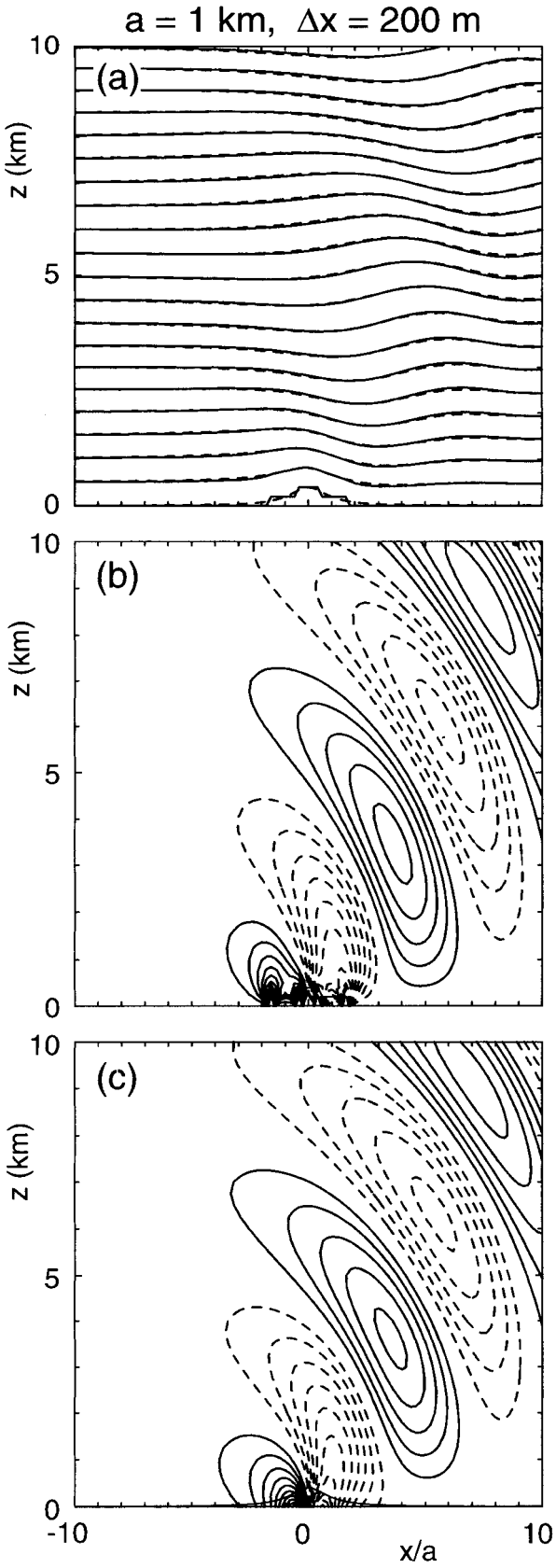

idealized mountain wave solutions for flow over a smooth barrier for a range of horizontal length scales that will produce both nonhydrostatic and hydrostatic responses.

One of the standard benchmark tests used for numerical models involves the simulation of inviscid 2D flow over a bell-shaped, or Witch of Agnessi, mountain defined by $h(x) = H/(1 + x^2/a^2)$ for an atmosphere that initially has wind speed U and Brunt–Väisälä frequency N that are constant with height. The steady mountain wave solution for this problem depends on three dimensionless parameters: NH/U, which reflects the nonlinearity of the flow; Na/U, which is a measure of the hydrostatic/nonhydrostatic influences; and fa/U (f being the Coriolis parameter), which reflects the importance of rotation. For small-amplitude mountains ($NH/U \ll 1$), the steady linear solution is known (cf. Queney 1948; Alaka 1960), and the structure of the waves depends on the mountain half-width a. For $Na/U \gg 1$ and $fa/U \ll 1$, hydrostatic waves are produced that are nondispersive. Wave energy and momentum propagate vertically and waves are confined to the region directly above the mountain, displaying lines of constant phase that tilt upstream with height. When the mountain width is smaller such that $Na/U = O(1)$, dispersive nonhydrostatic waves are produced that have horizontal and vertical lengths of similar magnitude. The horizontal group velocity is less than the phase speeds, resulting in an extension of the wave pattern downstream from the mountain. For $Na/U \ll 1$, the waves become evanescent and decay rapidly with height. For broad mountains with $fa/U = O(1)$, dispersive inertia–gravity waves are produced that again extend downstream from the mountain. For $fa/U \gg 1$, the waves become quasigeostrophic and decay rapidly with height.

In this study, we shall consider both analytic solutions and numerical simulations for flow over a bell-shaped mountain that is approximated by steps of height Δz that are regulated by the vertical resolution. We begin in section 2 by deriving the linear analytic solution for a single top hat mountain, and then construct approximations to the bell profile by adding together the steps for each grid level. In section 3, we present numerical simulations for mountain widths in both the nonhydrostatic and hydrostatic regimes that confirm the predictions of the analytic theory. Sensitivity of these results to both horizontal and vertical resolution will be examined. In section 4, we summarize the results and

←

FIG. 1. Linear step-terrain mountain solution for a narrow bell-shaped mountain ($a = 1$ km). Vertical resolution is $\Delta z = 0.5H$, horizontal resolution is $\Delta x = 0.2a = 200$ m. (a) Steady streamlines (solid lines) are displayed together with streamlines for the continuous bell-shaped mountain (dashed lines). Vertical velocity for (b) step terrain and for (c) the actual bell-shaped mountain are displayed with a contour interval of 0.25 m s^{-1}.

comment on their implications for more complex high-resolution prediction models.

2. Linear theory of flow over a step mountain

In 1943 Lyra derived the analytic solution for flow over a top hat–shaped mountain (see Alaka 1960). Rederiving this solution for an atmosphere that includes rotation, we seek solutions of the steady wave equation written in terms of the Fourier transform of the displacement $\delta = \sqrt{(\rho_0/\overline{\rho})}\,\delta_1$ that is well approximated by

$$\frac{\partial^2 \hat{\delta}_1}{\partial z^2} + \ell^2 \hat{\delta}_1 = 0, \qquad \ell^2 = \frac{N^2}{U^2}\frac{[1 - (kU/N)^2]}{[1 - (f/kU)^2]}, \quad (1)$$

where k is the horizontal wavenumber, $f = 10^{-4}$ is the Coriolis parameter, and the factor $\sqrt{\rho_0/\overline{\rho}}$ represents the growth in amplitude that arises due to the vertical variation in mean density $\overline{\rho}$. Within the expression for ℓ^2, the bracketed term in the numerator reflects the nonhydrostatic contribution to the solution while the bracketed term in the denominator represents the influence of the Coriolis force. For a top hat mountain with $h(x) = H$ for $|x| \le a_t$, $\delta(k, 0) = (2H/a_t)\sin ka_t$, which together with a wave radiation upper boundary condition yields a solution to (1) of the form

$$\hat{\delta}_1(k, z) = \frac{2H}{k}\sin ka_t \begin{cases} \exp[i\,\mathrm{sgn}(k)\ell z], & \text{for } \ell^2 > 0, \\ \exp(-\mu z), & \text{for } \ell^2 \le 0, \end{cases} \quad (2)$$

where $\mu = \sqrt{-\ell^2}$. Taking the inverse Fourier transform of (2) results in the following integral expression for the displacement of steady nonhydrostatic waves:

$$\delta(x, z) = \frac{2H}{\pi}\left(\frac{\rho_0}{\overline{\rho}}\right)^{1/2}\left\{\int_0^{f/U} \frac{\sin ka_t}{k}\exp(-\mu z)\cos kx\, dk + \int_{f/U}^{N/U} \frac{\sin ka_t}{k}\cos[kx + \ell z]\, dk + \int_{N/U}^{\infty} \frac{\sin ka_t}{k}\exp(-\mu z)\cos kx\, dk\right\}. \quad (3)$$

This equation can then be integrated numerically to obtain the displacement height of streamlines passing over a single top hat mountain of half-width a_t. To compute the solution for a step-terrain profile that approximates the bell-shaped mountain for specified grid increments Δx and Δz, we discretize the terrain profile into a series of steps on the specified grid and solve (3) in each vertical layer for a top hat profile of height Δz and width $2a_t$ of the step-terrain at that level. Summing the displacements produced by the step at each level then yields the linear solution for the multilevel step-terrain mountain profile.

In order to more directly compare the analytic results to integrations of the discretized model equations, we recast the above equations in finite difference form to account for the finite resolution resulting from the specified Δx. Representing the Fourier integral by a finite sum over wavenumbers $k = 2n\pi/x_l$ for $0 \le n \le N$, where $N = x_l/(2\Delta x)$, the solution for δ becomes

$$\delta(x, z) = \frac{4H}{x_l}\left(\frac{\rho_0}{\overline{\rho}}\right)^{1/2} \times \left[\frac{a_t}{2}\cos\frac{Nz}{U} + \sum_{n=1}^{m_1}\frac{\sin ka_t}{k}\exp(-\mu z)\cos kx + \sum_{n=m_1+1}^{m_2}\frac{\sin ka_t}{k}\cos(kx + \ell z) + \sum_{n=m_2+1}^{N}\frac{\sin ka_t}{k}\exp(-\mu z)\cos kx\right], \quad (4)$$

where m_1 is the largest n satisfying $k \le f/U$, m_2 is the largest n satisfying $k < N/U$, and x_l is the assumed domain size, which for $x_l \gg a$ has little impact on the solution. The vertical velocity $w = U\delta_x$ is obtained from the x derivative of (4).

a. Analytic step-terrain solutions at various horizontal scales

We consider first a case in the nonhydrostatic regime by setting $N = 10^{-2}$ s^{-1}, $U = 10$ m s^{-1}, for a bell-shaped mountain with $a = 1$ km, such that $aN/U = 1$. In this situation, vertically propagating disturbances above the step corners are comparable in horizontal scale to the scale of the mountain; artificial perturbations near the grid scale that are produced above the step corners are evanescent and decay rapidly with height. Even with a coarse vertical resolution of the terrain ($\Delta z = H/2$; i.e., the bell-shaped mountain is represented as two steps) the solution agrees favorably with the analytic solution for the actual bell-shaped mountain, as reflected by the steady streamlines in Fig. 1a and vertical velocity in Figs. 1b and 1c. Here, the horizontal grid interval is fixed at $\Delta x = 0.2a = 200$ m. The step-terrain results are rather insensitive to horizontal resolution, although peak magnitudes are increased somewhat with higher horizontal resolution, producing greater departures from the solution for continuous terrain.

Increasing the bell-shaped mountain half-width to $a = 10$ km such that $Na/U = 10$ and $fa/U = 0.1$, the flow is nearly hydrostatic and rotational influences are small. In this regime, the disturbances generated above the corners are small in horizontal scale compared to the mountain width. For $\Delta z = 0.5H = 200$ m and $\Delta x = 0.2a = 2$ km, these corner disturbances have amplitudes that are comparable to the mountain scale perturbation and appear as noise in the streamline field (Fig. 2a) and as vertically stacked oscillations above each corner in the vertical velocity field (Fig. 2b). Increasing the vertical resolution to $\Delta z = 0.1H = 40$ m, the corner disturbances are diminished in amplitude; the stream-

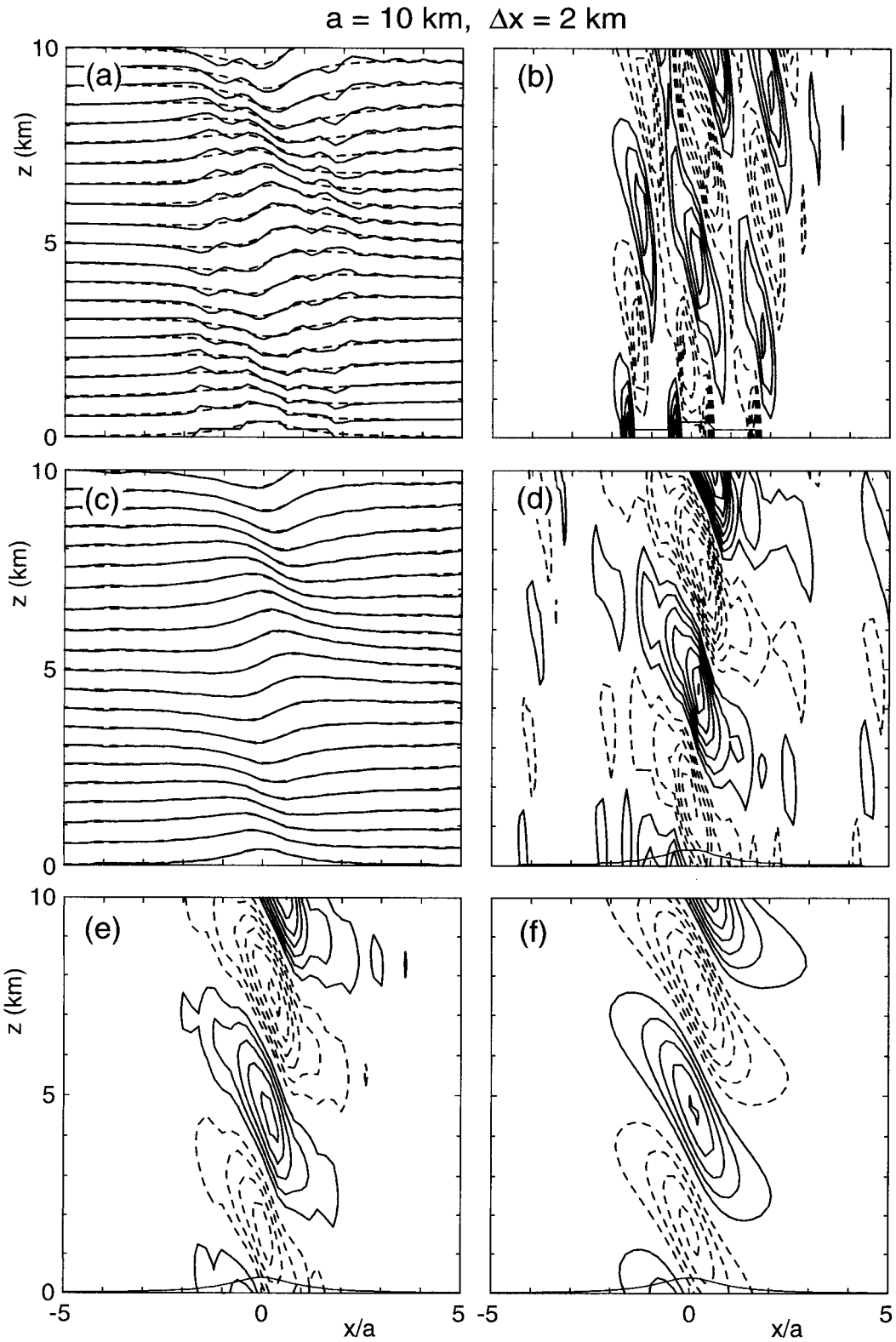

FIG. 2. Linear step-terrain mountain solution for a bell-shaped mountain with half-width $a = 10$ km. Horizontal resolution is $\Delta x = 0.2a = 2$ km. (a) Steady streamlines (solid lines) for $\Delta z = 0.5H$ along with streamlines for the continuous bell-shaped mountain (dashed lines). (b) Vertical velocity for step-terrain mountain with contour interval 0.2 m s^{-1}. (c) Streamlines as in (a) except for $\Delta z = 0.1H$. (d) Vertical velocity as in (b) except for $\Delta z = 0.1H$ and with contour interval 0.1 m s^{-1}. (e) Vertical velocity as in (d) except for $\Delta z = H/40$. (f) Vertical velocity for the actual bell-shaped mountain, displayed with contour interval of 0.1 m s^{-1}.

lines exhibit only slight deviations from the bell-shaped mountain solution (Fig. 2c), although the vertical velocity field still contains noticeable distortion. At $\Delta z = H/40 = 10$ m, the streamlines (not shown) are indistinguishable from the bell-shaped mountain solution and the noise in w is of small amplitude (Fig. 2e).

For a broad mountain half-width of $a = 100$ km, $Na/U = 100$, and $fa/U = 1$, the flow will produce hydrostatic inertia–gravity waves above and downstream of the terrain. The horizontal scale of the disturbances above the step corners is now far smaller than the scale of the mountain, and for $\Delta z = 0.5H = 200$ m, their strong amplitude dominates the wave response (Figs. 3a,b). With increasing vertical resolution, the step-terrain solutions converge toward the bell-shaped mountain wave structure in similar fashion to the results shown for $a = 10$ in Fig. 2. At $\Delta z = 0.1H = 40$ m, the streamlines display little distortion while the vertical velocity still contains significant noise (Figs. 3c,d). Further increasing the vertical resolution to $\Delta z = H/40 = 10$ m, the streamlines (not shown) are coincident with the bell-shaped mountain solution and the w field (Fig. 3e) is approaching the bell-shaped mountain solution (Fig. 3f), although some noise in the solution is still apparent. For a given vertical resolution, increasing the horizontal resolution does not improve the solution; rather, the step-corner disturbances increase in amplitude and shrink in scale toward a discontinuity (Fig. 4).

b. Scale dependence of the step-corner disturbances

To better understand the nature of these step-corner disturbances, we consider first the behavior of hydrostatic flow in the absence of rotation (which has little influence on the corner disturbances). In this limit, $\ell = N/U$ and the middle term in (3) can be integrated from zero to infinity to produce a closed form expression for displacement:

$$\delta(x, z) = H\left(\frac{\rho_0}{\overline{\rho}}\right)^{1/2} \begin{cases} \cos\dfrac{N}{U}z + \dfrac{1}{\pi}\ln\left|\dfrac{x - a_t}{x + a_t}\right| \sin\dfrac{N}{U}z, \\ \quad \text{for } |x| < a_t, \\ \dfrac{1}{\pi}\ln\left|\dfrac{x - a_t}{x + a_t}\right| \sin\dfrac{N}{U}z, \\ \quad \text{for } |x| > a_t. \end{cases} \tag{5}$$

Thus, for hydrostatic waves, a logarithmic singularity exists above each step corner that is independent of height. As long as the horizontal resolution remains within the hydrostatic regime, decreasing Δx only serves to increase the amplitude of the corner disturbances by better resolving this logarithmic singularity (as in Fig. 4).

In spite of the singular nature of hydrostatic disturbances above a step corner, as reflected in (5), the numerical representations of these disturbances remain finite for a fixed horizontal resolution, and diminish in amplitude with increasing vertical resolution, as demonstrated in Fig. 3. To understand this behavior, note that the singularity in (5) comes from the k^{-1} factor in the middle term of (4), evaluated in the hydrostatic limit. For a fixed horizontal grid, k is limited in magnitude by an upper bound of $\pi/\Delta x$. Thus, for a fixed Δx, the amplitude above the corners remains finite. Since the magnitude of the corner disturbance in (5) is proportional to the height of the step H, increasing the vertical resolution (decreasing the height of each step) decreases the amplitude of the corner disturbance.

In the nonhydrostatic regime, the singularity above a step corner is removed (except right at the corner point) due to the dispersive behavior of the waves. In fact, the disturbances above a step corner are described by the solution for flow over a wide plateau, as derived by Lyra (see Alaka 1960). One must exercise caution in interpreting solutions for flow over a semi-infinite plateau since the horizontal velocity perturbations actually become logarithmically infinite (cf. Bretherton 1969). However the vertical velocity field is well behaved and can be viewed as the asymptotic solution for a very wide (but not infinite) plateau. This solution can be readily obtained from (4) specifying a large value of a_t. Figure 5a displays the w field for a step plateau of height $H = 200$ m, obtained with $\Delta x = 200$ m. At this grid size the nonhydrostatic wave response is well resolved. With coarser resolution ($\Delta x = 2$ km), this wave response is marginally resolved (Fig. 5b) and is nearly identical to the perturbations above the leftmost step corner in Fig. 2b. These results for a step plateau confirm that the disturbances above each step corner would be nonhydrostatic waves if well resolved, but appear as spikes in the solution for coarser grids, and approximate a singularity if the resolved horizontal scales are essentially hydrostatic.

3. Model simulations

To evaluate the step-terrain approximation in numerical simulations of flow over a bell-shaped mountain, we employ a two-dimensional nonhydrostatic version of the NCEP Eta Model (Gallus and Rancic 1996). The Eta advection schemes (Janjic 1984) were replaced in these experiments with the third-order accurate Takacs (1985) scheme used in the thermal bubble tests by Gallus and Rancic (1996).

In the simulations that follow, the atmospheric conditions are the same as described in the previous section, which are also patterned after those used in tests with the Mesoscale Model version 5 (MM5) terrain-following model (Dudhia 1993). Thus, U is chosen to be 10 m s^{-1}, a bell-shaped terrain profile is specified with $H = 400$ m, and the constant Brunt–Väisälä frequency is $N = 10^{-2}$ s^{-1}. Three mountain half-widths are used, $a = 1$ km, 10 km, and 100 km, with a horizontal grid size of $0.2a$ for direct comparison with the analytic re-

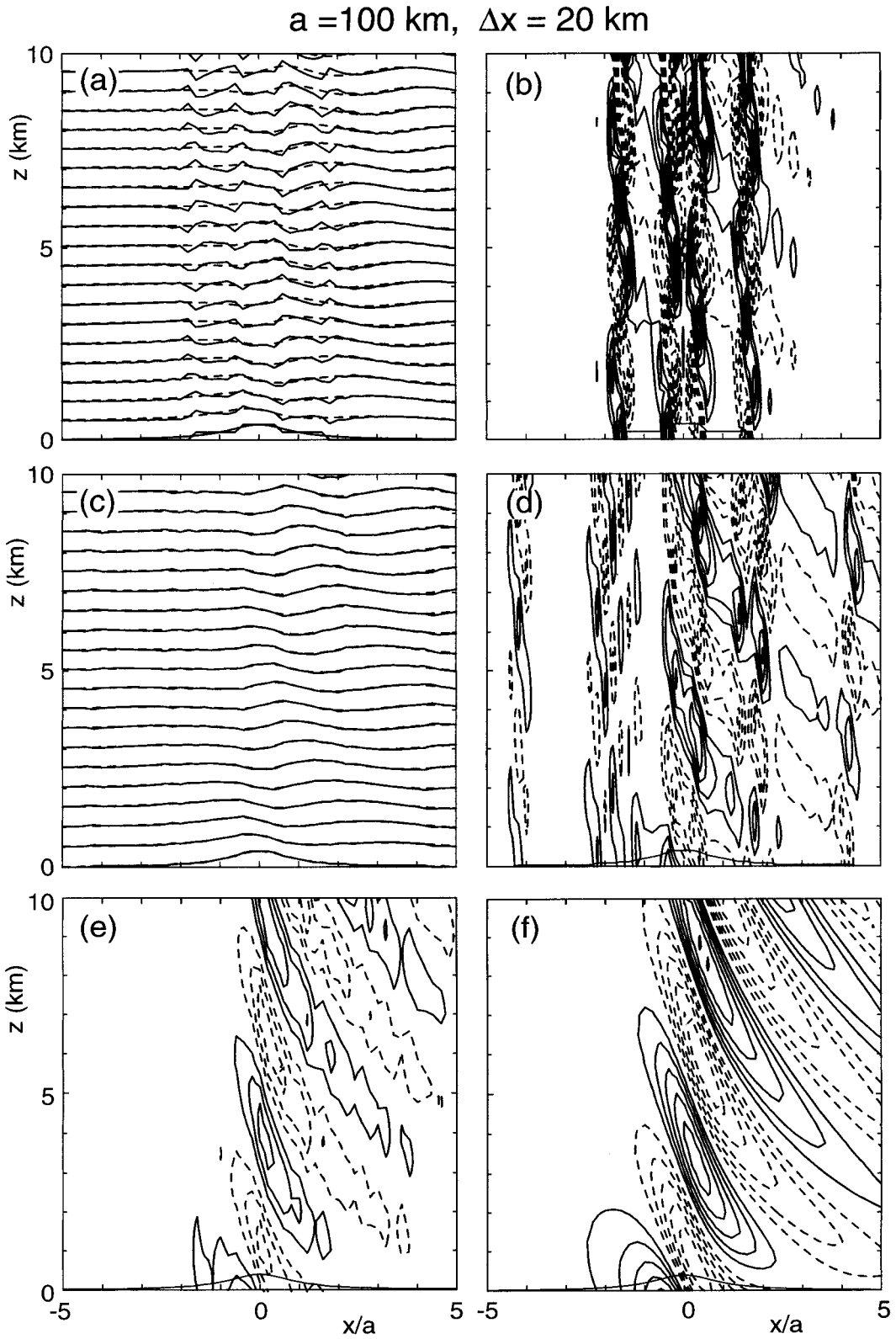

FIG. 3. As in Fig. 2 except a = 100 km, with $\Delta x = 0.2a = 20$ km. Contour interval is (b) 0.02 m s^{-1}, (d), (e) 0.01 m s^{-1}, and (f) 0.005 m s^{-1}.

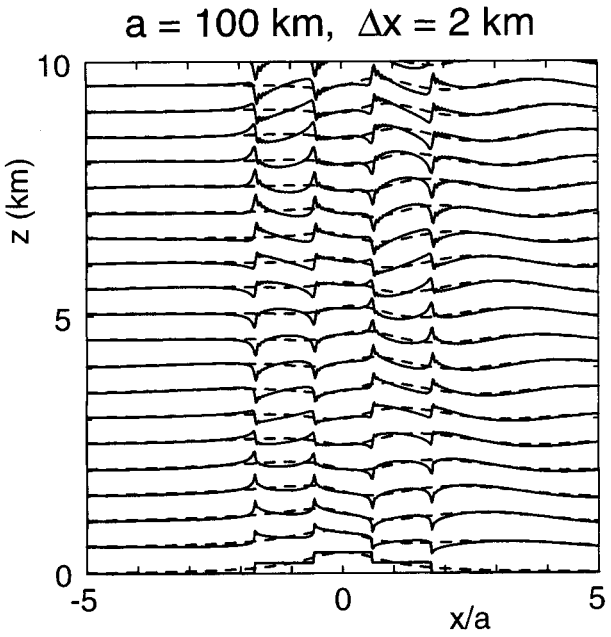

FIG. 4. As in Fig. 3a except with $\Delta x = a/50 = 2$ km.

sults in the previous section and Dudhia's MM5 simulations. The model top is at ~15.6 km (100 mb), with a Rayleigh damping absorbing layer (following Durran and Klemp 1983) beginning above 9 km to absorb upward propagating gravity wave energy. Simulations were performed with vertical resolutions ranging from 200 to 10 m (mountain represented from 2 to 40 steps). The horizontal domain width is $40a$, with open radiation boundary conditions specified at the lateral boundaries. The simulations were integrated for $21.6a/U$ s as in Dudhia (1993).

The hydrostatic version of the model was also run for all experiments as a test of the validity of the nonhydrostatic version of the code. As expected, results were nearly identical for the $a = 10$ and 100 km experiments, with significant differences arising for $a = 1$ km where nonhydrostatic effects are important. (In the hydrostatic model, the results for $a = 1$ km are qualitatively similar to those for $a = 10$ km but with greater amplitudes for the perturbations vertically stacked above the mountain).

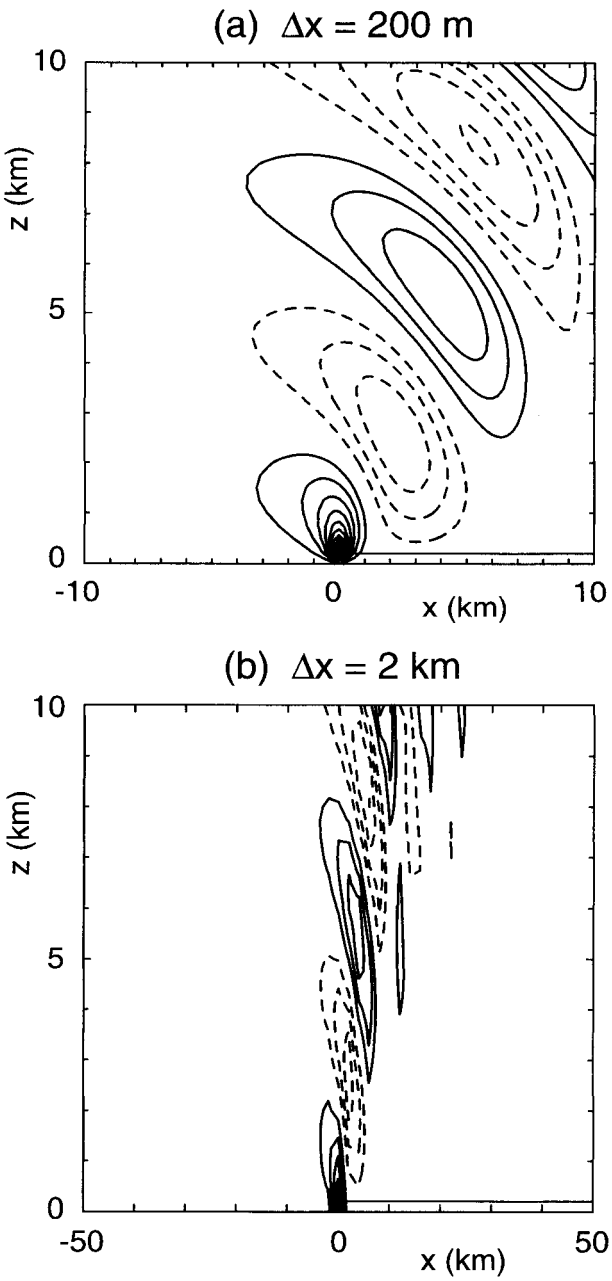

FIG. 5. Vertical velocity from linear solution for flow over a step plateau of height $H = 200$ m. Contour interval is 0.2 m s^{-1}. Solution is computed with (a) $\Delta x = 200$ m and with (b) $\Delta x = 2$ km.

a. Flow separation at step corners

When the model was run as originally configured, a fundamental discrepancy from the analytic solutions arose in the numerical results as flow separation developed at low levels in the lee of the mountain. This region of nearly stagnant flow is clearly apparent in the perturbation wind field shown in Fig. 6a, but does not appear either in analytic solutions for the true bell-shaped mountain, or in terrain-following models used in Witch of Agnesi experiments. The artificial response occurs in the step-terrain model independent of the vertical resolution; the effect is not removed (or even reduced) with a small vertical grid size. The region of nearly stagnant flow that develops downwind of the mountain effectively alters the shape of the forcing and greatly reduces the amplitude of the waves aloft.

We believe the flow separation above the lee slope arises in step-terrain models due to the artificial generation of significant horizontal (y component) vorticity ($\zeta_y = \partial u/\partial z - \partial w/\partial x$) at the step corners (Fig. 6b). Although there should be no vorticity generation along the

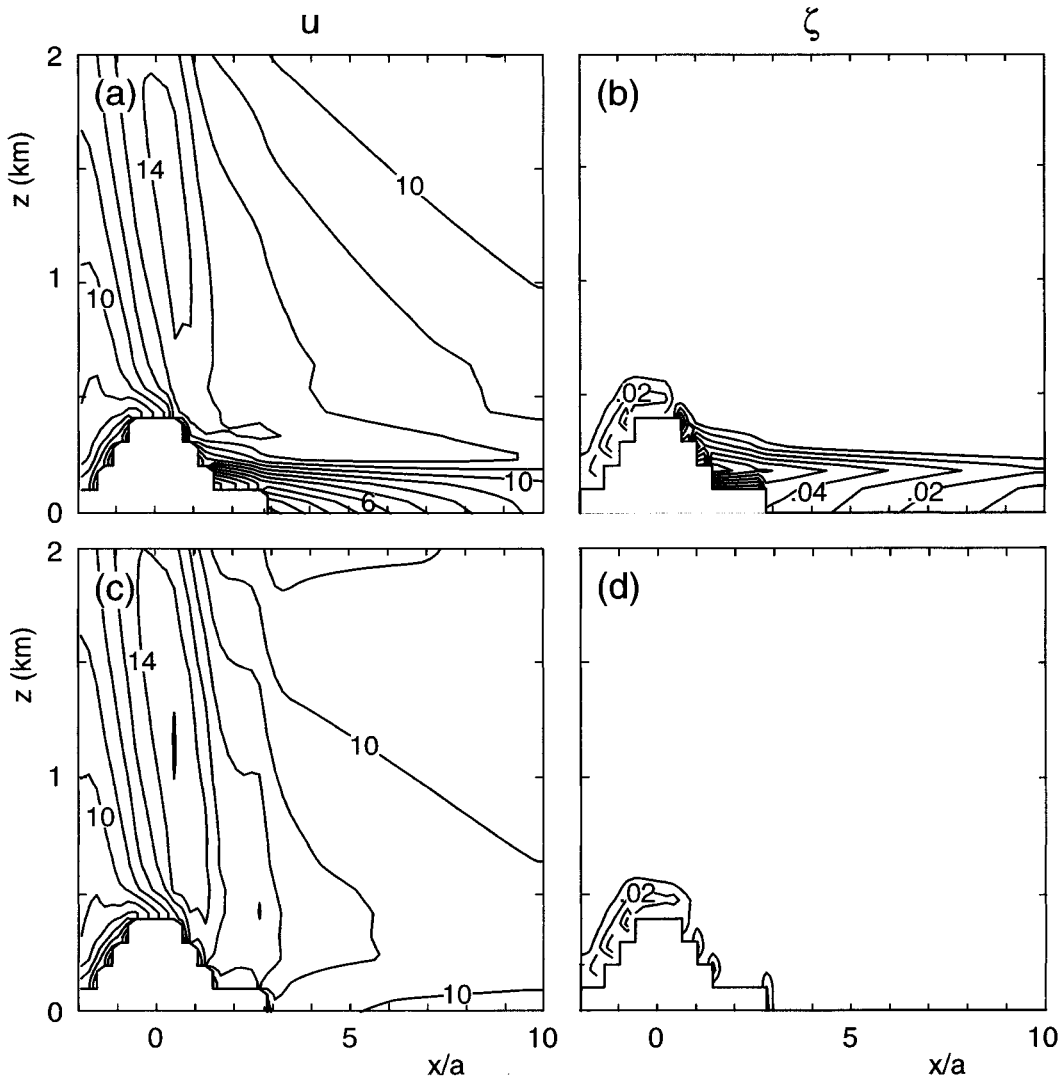

FIG. 6. Values of (a) horizontal velocity and (b) *y*-component horizontal vorticity ($\partial u/\partial z - \partial w/\partial x$) from a nonhydrostatic Eta Model simulation at $t = 2160$ s for step-terrain representation of a bell-shaped mountain of height $H = 400$ m and half-width $a = 10$ km with $\Delta x = 2$ km and $\Delta z = 100$ m without vorticity modification at the step corners. Horizontal velocity and *y*-component horizontal vorticity are shown in (c) and (d), respectively, for the same simulation with vorticity modification near step corners. (a), (b) Note flow separation downwind of the mountain and large values of vorticity at step corners. (a) and (c) Contour interval of 1 m s^{-1} and (b) and (d) 0.01 s^{-1}.

terrain surface for inviscid flow (if baroclinic generation is negligible), the singularity at the step corners creates an indeterminacy that is reflected in the solution by the generation of vorticity at the step corner. One can imagine a whole spectrum of different solutions that might arise, each corresponding to a different amount of vorticity generation at the corners.

To replicate the behavior of inviscid flow over smooth terrain, we seek model solutions in which there is no generation of vorticity at the step corners. After investigating several alternative approaches, we found that a simple application of a $\zeta_y = 0$ condition at each corner point was most effective at removing the lee-slope separation. With the C-grid staggering, this corner condition alters the finite differences used in the advection terms at the *u* and *w* points immediately above and beside the step corners, respectively. In other words, for the *u* point located one-half grid point above the step corner, vertical advection at the corner was computed as $\overline{w}^x \partial w/\partial x$ instead of using $-\overline{w}^x \partial u/\partial z$. Likewise, for the *w* point adjacent to the step corners, horizontal advection at the corner was computed using $\overline{u}^z \partial u/\partial z$ instead of $-\overline{u}^z \partial w/\partial x$. (Here, the overbars indicate averaging of values on either side of the corner point that is located in between both the *u* and *w* grid locations.) It is acknowledged that this alteration is probably too restrictive since, in general, the horizontal vorticity along the surface does not vanish; it may be present in

the mean flow due to wind shear or baroclinically generated within the perturbed flow. However, it does serve to eliminate most of the flow separation by diminishing or preventing vorticity generation at the step corners (see Figs. 6c,d) and appears to work better than other more sophisticated alterations we investigated (e.g., permitting mass to flow into and out of grid boxes having a step face). Therefore, this alteration was used in the simulations discussed in the following section.

b. Step-terrain simulations at various horizontal scales

For a mountain half-width of 1 km, the most strongly forced stationary wave modes have horizontal and vertical wavelengths of similar magnitude, and thus the waves are strongly nonhydrostatic. Vertical velocity perturbations in the analytic solution display wave fronts propagating upward and downstream as shown in Fig. 1c. Similar results are obtained from the nonhydrostatic Eta Model with a vertical resolution of 200 m that only coarsely represents the bell-shaped mountain with a two-layer step-terrain profile (Fig. 7a) and also with a finer vertical resolution of 10 m (Fig. 7b). For these nonhydrostatic waves, the perturbations above the step corners are well resolved for $\Delta x = 0.2a$ (cf. Fig. 5a), and thus, the solution is not affected appreciably by further increasing the horizontal resolution. These results agree well with those from both the analytic bell-shaped mountain solution (Fig. 1c) and its step-terrain approximation (Fig. 1b). Small-scale extrema do occur near the step corners, but the dispersive nature of the waves causes the grid-scale perturbations to disappear rapidly with height. Only the lowest few hundred meters appear distorted by the step corners.

With a mountain half-width of 10 km, hydrostatic mountain waves dominate and rotational effects are unimportant. Vertical velocity perturbations in the analytic bell-shaped mountain solution (Fig. 2f) show that little propagation downstream occurs, unlike the case with nonhydrostatic waves. A series of perturbations of alternating sign are vertically stacked above the mountain. In the step-terrain model, significant vertical perturbations occur above each step corner in the coarse vertical resolution simulation using $\Delta z = 200$ m (Fig. 8a). This behavior is quite similar to the perturbations evident in the analytic two-layer step-terrain solution in Fig 2b, and reveals a composite of step-corner disturbances similar to the one isolated in Fig. 5b. When the vertical resolution is improved to 10 m, the amplitude of the step-corner perturbations decreases significantly (Fig. 8b). Perturbations in w are now in good agreement with the analytic bell-shaped mountain solution (Fig. 2f), with only slight distortion due to the corner effects.

For a half-width of 100 km, with a horizontal resolution of 20 km, the step-terrain Eta Model displays a similar behavior to that discussed for the 10-km half-width mountain. Again, artificial perturbations above the step corners dominate the vertical velocity field for $\Delta z = 200$ m (Fig. 9a). With significantly higher vertical resolution $\Delta z = 10$ m, the simulation (Fig. 9b) approaches the analytic solution for the bell-shaped mountain (Fig. 3f), although the model appears to be converging to this result more slowly with increasing vertical resolution than the analytic step-terrain solutions (Figs. 3a–e). The secondary extrema seen near the right edge of the domain in Fig. 9b shifted in position and were reduced somewhat in magnitude in a sensitivity test in which varying vertical resolution was used, allowing the mountain to be resolved in even greater detail by steps of height 1 m (lowest levels) to 6 m (moun-

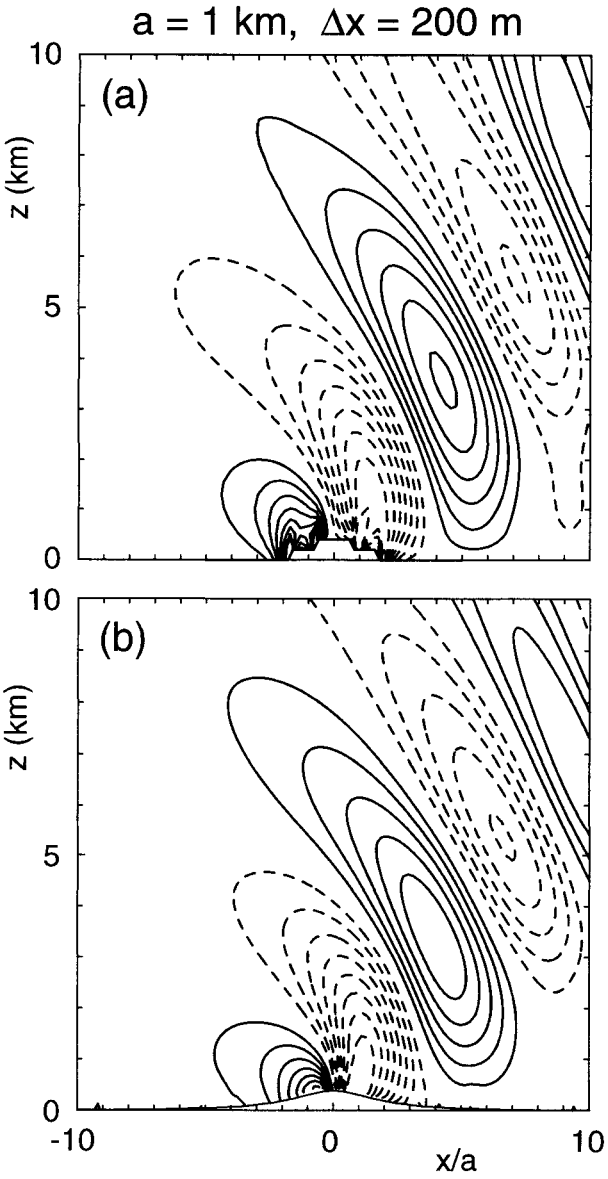

FIG. 7. Vertical velocity from nonhydrostatic Eta Model simulations with a mountain half-width of 1 km (horizontal resolution of 200 m), with vertical resolution of Δz = (a) $0.5H$ = 200 m and (b) $H/40$ = 10 m. Contour interval is 0.25 m s^{-1}.

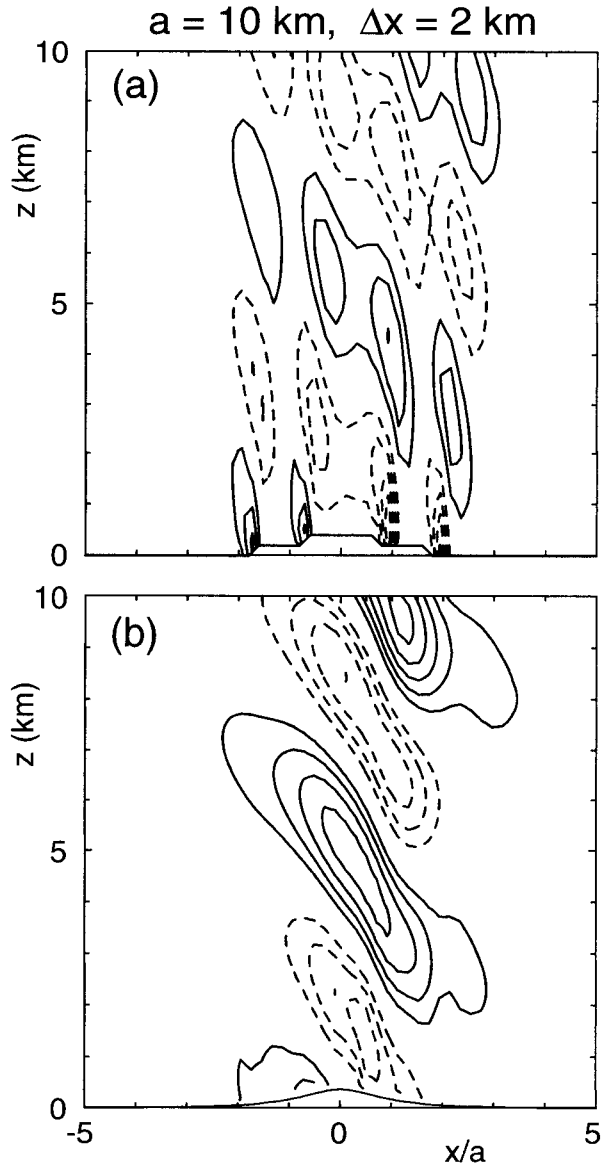

FIG. 8. As in Fig. 7 except for a mountain half-width of 10 km (horizontal resolution of 2 km). (a) Contour interval is 0.2 m s^{-1} and (b) 0.1 m s^{-1}.

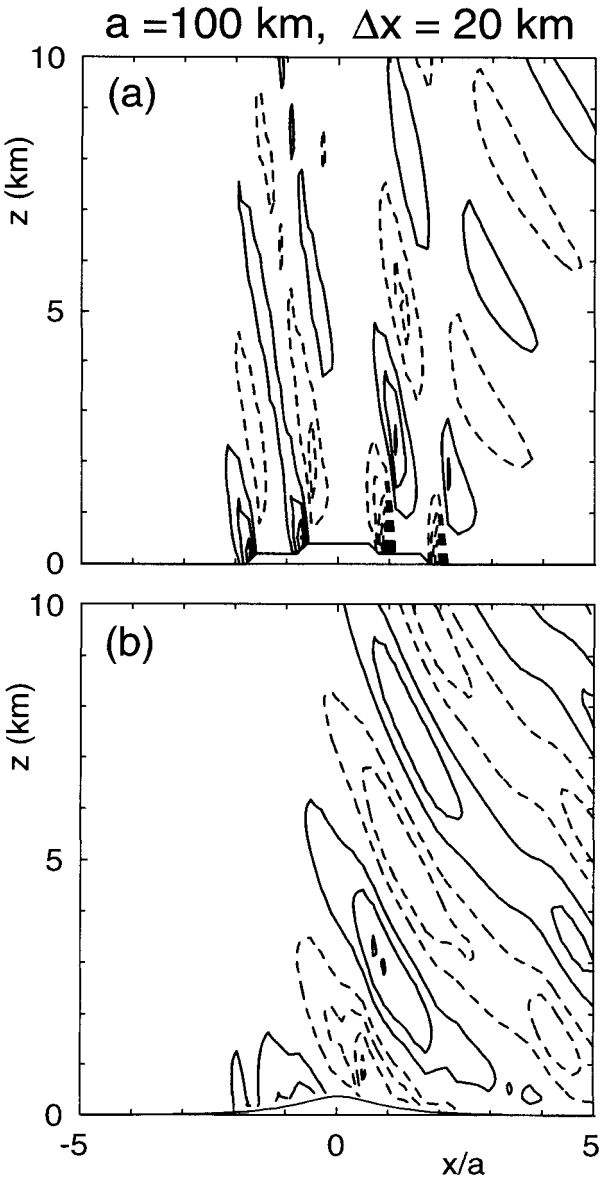

FIG. 9. As in Fig. 7 but for a mountain half-width of 100 km (horizontal resolution of 20 km). Contour interval is (a) 0.02 m s^{-1} and (b) 0.01 m s^{-1}.

taintop). This result suggests that the simulation would approach the analytic solution if extremely high vertical resolution were used.

4. Discussion

In this investigation, we have evaluated the viability of using a step-terrain representation of a smooth mountain profile in model simulations of small-amplitude mountain waves, where results can be compared against known analytic solutions. Both the analytic solutions and simulations with a 2D nonhydrostatic version of the NCEP's regional Eta Model demonstrate that the accuracy of the step-terrain approximation may depend strongly on the horizontal scale of the terrain and the resolution of the actual terrain by the vertical grid. According to linear theory, the steady-state disturbance produced by a single step is nonhydrostatic and has a structure as illustrated in Fig. 5. When the horizontal scale of the mountain is comparable to the scale of the disturbance produced above the individual step corners, the step-terrain approximation to a smooth mountain profile may produce a reasonable wave response (except near the step corners) even with rather coarse resolution of the actual terrain. In this situation, superposition of the circulation above each step corner may combine to produce a continuous wave response that approximates

the wave structure above the actual continuous slope. However, in simulations of nearly hydrostatic waves, more significant distortions may arise since the scale of disturbances generated above the step corners is much smaller than the scale of the mountain forcing, and consequently, the circulation above each step corner appears as a localized spike in the flow field. While the amplitude of the disturbances above the corners is independent of the mountain width, the vertical velocity in the mountain-scale wave decreases in proportion to increases in the mountain width. Thus, the relative amplitude of these step-corner disturbances becomes increasingly dominant as the mountain width increases. In the hydrostatic limit, the analytic solutions reveal that a logarithmic singularity exists at all heights above each step corner but that the numerical representations remain finite for a fixed horizontal grid.

In applications where the wave response is not strongly nonhydrostatic, the vertical grid size must be small enough to accurately approximate the actual shape of the terrain. This requirement that $\Delta z \ll H$ is far more restrictive than the resolution needed to resolve the wave structure aloft (i.e., $\Delta z \ll 2\pi U/N$) since the vertical length is typically at least an order of magnitude greater than the mountain height. Both the analytic solutions (section 2) and model simulations (section 3) suggest that for a bell-shaped mountain of height $H = 400$ m, a vertical grid size of order 10 m is required to obtain an accurate representation of the gravity wave response for half-widths $a = 10$–100 km. In contrast, Dudhia (1993) obtained accurate simulations of flow over a bell-shaped mountain for these half-widths with a vertical grid of about 250 m near the surface (and becoming coarser aloft) using the traditional terrain-following coordinate.

For typical mesoscale horizontal resolutions (roughly 20 km) for research (e.g., Zhang and Gao 1989) or operational purposes (Black 1994), the amplitude of the mountain waves is sufficiently small that the step-corner perturbations may not significantly impact forecasts made with the models (except, of course, for the gravity waves themselves). In the simulation in section 3 for $a = 100$ km with $\Delta x = 20$ km and $\Delta z = 0.5H$, the perturbations associated with step corners are only several centimeters per second in magnitude. However, at cloud-scale resolutions of a few kilometers, these perturbations can be significantly greater. For the relatively small 400-m mountain simulated in section 3, for $a = 10$ km with $\Delta x = 2$ km and $\Delta z = 0.5H$, the peak artificial vertical velocity perturbations above the step corners are on the order of 0.5 m s^{-1}. Thus, in a real data situation with cloud-scale horizontal resolution, coarse vertical resolution could play a significant role in producing spurious vertical velocity forcing over large depths in the atmosphere. If such a pattern of ascent/descent is not eliminated by model damping, convection initiation might be artificially enhanced above the step corners.

In the current 32-km, 45-layer operational Eta Model (implemented in early 1998), the low-level vertical resolution generally varies from around 20 m in the lowest layer at sea level to around 125 m at 1000 m (Rogers et al. 1998). Vertical resolution near the top of the highest mountains (around 3000 m) is between 300 and 400 m. Experimental 10-km tests of the Eta Model have been run at NCEP using 60 layers with the coarsest vertical resolution at the highest mountains being around 300 m. The land surface and turbulence parameterizations in a step-terrain model will at least partially mask the effects of the step corners. However, as horizontal resolution is improved in future versions of step-terrain models like the Eta, care should be taken to maintain as high a vertical resolution as possible throughout layers where topography exists.

Idealized simulations with the 2D step-terrain model reveal a persistent tendency for the flow to separate above the lee slope of terrain features due to artificial horizontal vorticity generation at the step corners. This effect could be causing artificially weak flow in the lee of mountains in the operational Eta Model. There is a suggestion of this behavior in the operational 10-km Eta Model in a case of easterly flow over the Wasatch Mountains, documented by Staudenmaier and Mittelstadt (1997), in which the low-level flow failed to accelerate and descend along the lee slope. In practice, it appears that the spurious behavior in our idealized simulations can be greatly reduced or eliminated by specifying a zero vorticity condition at the corners (though this approach cannot be rigorously justified).

This study is not intended as a comprehensive evaluation of step-terrain and terrain-following coordinates over the entire spectrum of terrain situations. Most notably, we have not considered here their behavior for flow over and around steep mountains, for which the step-terrain representation may be more accurate and for which errors in computing the horizontal pressure gradient force in terrain-following coordinates may increase. Rather, we have focused on idealized flow over smooth orography to document the capabilities and limitations of the step-terrain representation in more controlled conditions. Further studies should include both more varied flow situations and more complex terrain. Additionally, the influence of boundary layer processes on the results, and three-dimensional effects, should be considered.

Acknowledgments. The first author would like to thank Miodrag Rancic for his assistance with the development of a nonhydrostatic version of the Eta Model. In addition, discussions with Tom Black, Joe Gerrity, Zavisa Janjic, and Fedor Mesinger were helpful. This work was sponsored by National Science Foundation–National Oceanic and Atmospheric Administration Grant ATM-9612388 to the USWRP program.

REFERENCES

Alaka, M. A., Ed., 1960: The airflow over mountains. WMO Tech. Note 34, 135 pp.

Black, T. M., 1994: The new NMC mesoscale Eta model: Description and forecast examples. *Wea. Forecasting,* **9,** 265–278.

Bretherton, F. P., 1969: Momentum transport by gravity waves. *Quart. J. Roy. Meteor. Soc.,* **95,** 213–243.

Bryan, K., 1969: A numerical method for the study of the circulation of the World Ocean. *J. Comput. Phys.,* **4,** 347–376.

Dudhia, J., 1993: A nonhydrostatic version of the Penn State–NCAR mesoscale model: Validation tests and simulation of an Atlantic cyclone and cold front. *Mon. Wea. Rev.,* **121,** 1493–1513.

Durran, D. R., and J. B. Klemp, 1983: A compressible model for the simulation of moist mountain waves. *Mon. Wea. Rev.,* **111,** 2341–2361.

Gal-Chen, T., and R. Somerville, 1975: On the use of coordinate a transformation for the solution of the Navier–Stokes equations. *J. Comput. Phys.,* **17,** 209–228.

Gallus, W. A., Jr., and M. Rancic, 1996: A nonhydrostatic version of the NMC's regional eta model. *Quart. J. Roy. Meteor. Soc.*, **122,** 495–513.

Janjic, Z. I., 1984: Nonlinear advection schemes and energy cascade on semi-staggered grids. *Mon. Wea. Rev.,* **112,** 1234–1245.

——, 1990: The step-mountain coordinate: Physical package. *Mon. Wea. Rev.,* **118,** 1429–1443.

——, 1994: The step-mountain eta coordinate model: Further developments of the convection, viscous sublayer, and turbulence closure schemes. *Mon. Wea. Rev.,* **122,** 928–945.

Mesinger, F., 1984: A blocking technique for representation of mountains in atmospheric models. *Riv. Meteor. Aeronaut.,* **44,** 195–202.

——, and Z. I. Janjic, 1985: Problems and numerical methods of incorporation of mountains in atmospheric models. *Large-Scale Computations in Fluid Mechanics,* Part 2, Lectures in Applied Mathematics, Vol. 22, Amer. Math. Soc., 81–120.

——, ——, S. Nickovic, D. Gavrilov, and D. G. Deaven, 1988: The step mountain coordinate: Model description and performance for cases of alpine cyclogenesis and for a case of an Appalachian redevelopment. *Mon. Wea. Rev.,* **116,** 1493–1518.

Phillips, N. A., 1957: A coordinate system having some special advantages for numerical forecasting. *J. Meteor.,* **14,** 184–185.

Queney, P., 1948: The problem of air flow over mountains: A summary of theoretical studies. *Bull. Amer. Meteor. Soc.,* **29,** 16–26.

Rogers, E., and Coauthors, 1998: Changes to the NCEP operational ''early'' eta analysis/forecast system. NWS Tech. Procedures Bull. 447, National Oceanic and Atmospheric Administration/ National Weather Service, 34 pp. [Available from National Weather Service, Office of Meteorology, 1325 East–West Highway, Silver Spring, MD 20910.]

Staudenmaier, M. J., and J. Mittelstadt, 1997: Results of the western region evaluation of the Eta-10 model. Western Region Tech. Attachment 97-18, 8 pp. [Available from National Weather Service Western Region-SSD, Rm. 1311, 125 S. State St., Salt Lake City, UT 84147; or online at http://nimbo.wrh.noaa.gov/wrhq/97TAs/TA9718/TA97-18.html.]

Takacs, L. L., 1985: A two-step scheme for the advection equation with minimized dissipation and dispersion errors. *Mon. Wea. Rev.,* **113,** 1050–1065.

Zhang, D.-L., and K. Gao, 1989: Numerical simulation of an intense squall line during 10–11 June 1985 PRE-STORM. Part II: Rear inflow, surface pressure perturbations and stratiform precipitation. *Mon. Wea. Rev.,* **117,** 2067–2094.